PHYSICAL REVIEW C VOLUME 17, NUMBER 3 MARCH 1978

Dynamics of induced fission*

J. W. Negele†
Center for Theoretical Physics, Massachusetts Institute of Technology, Cambridge, Massachusetts 02139

S. E. Koonin†
W. K. Kellogg Radiation Laboratory, California Institute of Technology, Pasadena, California 91125

P. Möller‡ and J. R. Nix
Theoretical Division, Los Alamos Scientific Laboratory, University of California, Los Alamos, New Mexico 87545

A. J. Sierk†
W. K. Kellogg Radiation Laboratory, California Institute of Technology, Pasadena, California 91125
and Theoretical Division, Los Alamos Scientific Laboratory, University of California, Los Alamos, New Mexico 87545§

(Received 18 October 1977)

Induced fission of ^{236}U is calculated in the time-dependent mean-field approximation assuming axial and reflection symmetry and omitting the spin-orbit interaction. Constrained static solutions are used to generate the appropriate initial condition and are compared in detail with results of macroscopic-microscopic calculations. Although dynamic mean-field results are strongly dependent upon an effective pairing gap, predicted observables are consistent with experiment for plausible values of the gap. Detailed comparisons with macroscopic models indicate that both a modified one-body dissipation and two-body viscosity yield observables similar to those of the mean-field theory, even though these physical dissipation mechanisms are fundamentally different.

[NUCLEAR REACTIONS, FISSION ^{236}U induced fission calculated in time-dependent mean-field approximation and with modified liquid-drop model. Comparison of dissipation mechanisms.]

I. INTRODUCTION

Fission dynamics provides an invaluable testing ground for nuclear many-body theory. Many of the crucial questions arising in heavy-ion reactions concerning dissipation mechanisms, the validity of fluid-dynamic and mean-field approximations, and the role of quantal effects are also relevant to fission. Given the availability of comprehensive, systematic fission data and the reasonably well developed state of computational technology, it is worthwhile to attempt to use fission as a definitive test of alternative theoretical approaches.

Microscopic many-body theory aspires to systematically calculate expectation values of relevant few-body operators in terms of the underlying two-body interaction. One possible starting point for a microscopic theory is the time-dependent mean-field approximation, usually referred to as the time-dependent Hartree-Fock (TDHF) approximation, which has been explored extensively in simplified slab geometry,[1] light-ion systems,[2-6] and analytically soluble models.[7,8] This approximation specifies the time evolution of the one-body density matrix, including the shape, surface thickness, interior density fluctuations, neck formation, and dissipation solely in terms of the effective two-body interaction and an initial condition. Since, in the case of induced fission, the appropriate initial condition is conceptually unambiguous, and because the theory is otherwise in principle independent of additional parametrizations or arbitrary phenomenological adjustments, one may hope to obtain a definitive test of the mean-field theory.

In the mean-field approximation, single-particle wave functions propagate in the nuclear interior like free wave packets in a constant potential, so dissipation and evolution of the nuclear shape arise from scattering from the edges of the self-consistent potential.[9] The crucial question, therefore, is whether this approximation describes the essential physics of fission or if the omitted two-particle–two-hole excitations are so important that the conspicuous single-particle behavior and suppression of scattering in the nuclear interior are grossly inaccurate oversimplifications. Experimental quantities with which we may compare the results of a general mean-field calculation include the mass asymmetry, mean values, and dispersion in fragment proton and neutron number, and the mean translational kinetic energies of fragments.

Macroscopic liquid-drop descriptions, in con-

trast, emphasize rather different physical aspects. Instead of attempting to formulate a theory which is uniquely specified by the two-body force, only very general features of the underlying interaction are invoked. One tacitly assumes that the force saturates at the proper density, that two-body collisions dominate so completely that local equilibration occurs throughout the medium, and that the forces give rise to a surface of the proper thickness. In this description, one is still free to explore alternative assumptions regarding viscosity or the presence of surface dissipation mechanisms. It is the opportunity for detailed comparisons of these alternative descriptions with each other and with experiment to distinguish between different physical mechanisms which motivated the investigations and comparisons presented in this work.

Unfortunately, practical limitations in implementing TDHF calculations have rendered the present investigation less definitive than is possible in principle.[9] In the first place, because of computational costs we have restricted our attention to the single nucleus ^{236}U, thereby giving up the constraints imposed by fission systematics. To the extent to which shell effects are unimportant, the systematics as a function of fissility could be explored in future work by simply varying the proton charge, greatly facilitating the calculation of the initial wave functions.

Second, because of the great computational savings effected by the imposition of symmetries, we have restricted the wave function to be axially and reflection symmetric. In contrast to the case of a general wave function, the single-particle Hamiltonian for an axially and reflection symmetric wave function does not connect single-particle states of different angular momentum projection and parity. Thus, in the mean-field theory, an axial and reflection symmetric wave function evolves only in an unreasonably restricted and completely unphysical subspace in which fission cannot occur at all. In this work, we have therefore used the constant-gap pairing approximation[10] as the simplest available mechanism to introduce matrix elements connecting states comprised of single-particle wave functions of differing parities or angular momentum projection. It must be understood from the outset that one deals with an effective gap or pairing strength which is intended to simulate the average effect of symmetry-breaking mean-field matrix elements, as well as the two-body residual interaction. Given that we are presently unable to derive the value of the effective gap, the present calculation therefore suffers from the introduction of one phenomenological parameter.

The final compromise arising from computational considerations is the omission of the spin-orbit force. This approximation accomplishes two major savings by avoiding the solution of sets of coupled equations for the spatial functions corresponding to the two spin projections and by decreasing the total number of spatial functions to be calculated and stored by almost a factor of $\frac{1}{2}$. As a result of this approximation, the single-particle shell effects in the ^{236}U fission barrier are totally unrealistic. To the extent to which induced fission is independent of shell effects, this limitation is inconsequential. Furthermore, comparisons with macroscopic calculations are not jeopardized by unrealistic shell effects, since the macroscopic theories neglect shell corrections altogether. However, we do give up the opportunity for exploring one of the key features of the microscopic theory: the interplay between single-particle and collective effects.

Thus, the present investigation is highly exploratory and falls short both of displaying the full capabilities of the mean field theory and of critically testing it to the fullest extent with available data.

II. TDHF APPROACH

A. Effective interaction

In contrast to the strict definition of TDHF, which would utilize the true two-body force, the time-dependent mean-field approximation requires the derivation of a suitable effective interaction. The interaction used in this work differs from that of Refs. 1 and 4 both with respect to isospin dependence and nonlocality. Guided by the fact that expansion of the exchange term of the nuclear density matrix and use of the Reid G matrix yields a Hamiltonian density very similar to that obtained with the Skyrme II and III interactions,[11] we utilize the following form for the Hamiltonian functional[12]:

$$\mathcal{H}=\int d^3r\left(\frac{\hbar^2}{2m}(\tau_n+\tau_p)+\frac{\tilde{t}_0}{2}[(2+\tilde{x}_0)\rho_n\rho_p+\frac{(1-\tilde{x}_0)}{2}(\rho_n^2+\rho_p^2)]+\frac{t_1+t_2}{4}[(\rho_n+\rho_p)(\tau_n+\tau_p)-(J_n+J_p)^2]\right.$$
$$\left.+\frac{t_2-t_1}{8}(\rho_n\tau_n-J_n^2+\rho_p\tau_p-J_p^2)+\frac{t_3}{4}(\rho_n\rho_p^2+\rho_p\rho_n^2)\right)+\frac{v_L}{2}[E_Y(\rho_n,\rho_n)+E_Y(\rho_p,\rho_p)]+v_U E_Y(\rho_n,\rho_p)+E_C\,, \quad (1)$$

where the direct Coulomb contribution is

$$E_C(\rho_p)=\frac{e^2}{2}\int\int d^3r d^3r'\frac{\rho_p(\vec{r})\rho_p(\vec{r}')}{|\vec{r}-\vec{r}'|} \quad (2)$$

and the direct Yukawa contribution is

$$E_Y(\rho_q,\rho_{q'})=\int\int d^3r d^3r'\frac{e^{-\mu|\vec{r}-\vec{r}'|}}{\mu|\vec{r}-\vec{r}'|}\rho_q(\vec{r})\rho_{q'}(\vec{r}'). \quad (3)$$

The densities ρ and τ are defined by

$$\rho(\vec{\mathbf{r}}) = \sum_i \eta_i |\psi_i(\vec{\mathbf{r}})|^2 \tag{4a}$$

and

$$\tau(\vec{\mathbf{r}}) = \sum_i \eta_i |\nabla\psi_i(\vec{\mathbf{r}})|^2, \tag{4b}$$

and the current is

$$\vec{J}(\vec{\mathbf{r}}) = \sum_i \eta_i \, \mathrm{Im}\psi_i^*(\vec{\mathbf{r}})\nabla\psi_i(\vec{\mathbf{r}}), \tag{4c}$$

where η_i denotes the occupation probability of the ith single-particle wave function. Since calculations with realistic interactions[11] yield a nonlocality corresponding to an effective mass $m^*/m \approx 0.6$, the $\rho\tau - J^2$ terms are taken over directly from the Skyrme force. The isospin dependence of the Skyrme force is also included, since we now address ^{236}U, which has a large neutron excess. Because there is no real advantage in expanding the finite-range direct terms in the Skyrme form, we have retained explicit finite-range Yukawa forces as in Refs. 1 and 4. Given the form of Eq. (1) and the Yukawa range of Ref. 4, a unique correspondence with a set of Skyrme parameters may be established by requiring that a Taylor-series expansion of the Yukawa term $E_Y(\rho_q, \rho_{q'})$ exactly reproduce the coefficient of $\rho_q\nabla^2\rho_{q'}$ in the Skyrme Hamiltonian, Eq. (12) of Ref. 13. This yields the relations

$$2\pi v_L = \frac{3\mu^5}{32}(t_1 - t_2) \tag{5a}$$

and

$$4\pi v_U = \tfrac{1}{8}\mu^5(t_2 - 3t_1), \tag{5b}$$

where t_1 and t_2 are Skyrme parameters. The first term in the expansion of $E_Y(\rho_q, \rho_{q'})$ corresponds to a δ function, so that the volume integrals of the Yukawa functions must be removed from the zero-range components:

$$\frac{\tilde{t}_0}{4}(1 - \tilde{x}_0) = \frac{t_0}{4}(1 - x_0) - \frac{2\pi v_L}{\mu^5} \tag{6a}$$

and

$$\frac{\tilde{t}_0}{2}(2 + \tilde{x}_0) = \frac{t_0}{2}(2 + x_0) - \frac{4\pi v_U}{\mu^5}. \tag{6b}$$

The parameters thus obtained from the Skyrme II and Skyrme III interactions are tabulated in Table I. By construction the corresponding Yukawa and Skyrme forces yield identical results in nuclear matter, and differ negligibly in heavy nuclei. Except when indicated otherwise, all calculations were performed with interaction II of Table I. Constrained static calculations of the fission barrier were also carried out with interaction III, and the negligible differences in the barrier shapes indicate that the two interactions are equivalent for our present purposes.

TABLE I. Modified Skyrme parameters appearing in Eq. (1).

Force	$\tilde{t}_0$ (MeV fm^3)	$\tilde{x}_0$	μ (fm^{-1})	v_U (MeV)	v_L (MeV)
II	−104.49	4.01	2.175	−868.53	−444.85
III	−334.47	1.743	2.175	−619.60	−355.79

B. Initial conditions

In induced fission, the initial conditions for our dynamical calculations may be determined conveniently by means of the transition-state method.[14,15] In this method one first determines the normal modes of the system at its saddle point and then divides the original system of N degrees of freedom into two systems: a system with a single degree of freedom representing unstable motion in the fission direction, and a second system with $N-1$ degrees of freedom representing stable motion in the nonfission directions.

The standard assumption of the transition-state method is that statistical equilibrium is established by the time the system arrives in the vicinity of its saddle point. This assumption should be valid because a compound nucleus undergoing fission typically executes about 10^6 oscillations between formation and reaching the saddle point, which provide ample opportunity for many interchanges of energy. From this assumption one may calculate the probability that when the nucleus passes through the vicinity of its saddle point each of the normal coordinates are displaced from their equilibrium values by given amounts and that their conjugate momenta have specified values.

At high excitation energies, where classical statistical mechanics is valid, this probability is given by the usual Boltzmann factor evaluated at the saddle point. This leads in the harmonic approximation to Gaussian probability distributions in each of the normal coordinates and momenta, with widths proportional to the square root of the nuclear temperature at the saddle point. For the $N-1$ normal coordinates and momenta representing bounded motion, the probability in the harmonic approximation remains Gaussian also through intermediate excitation energies down to zero excitation energy at the saddle point.[14,15] In the latter limit the widths of the distributions are determined by quantal zero-point oscillations. However, for the fission normal coordinate, the probability has been worked out only in the classical

limit.

From this discussion, it is evident that one should ideally sample an ensemble of initial conditions corresponding to the distribution of configurations occurring at the saddle point. A conceivable microscopic framework for such a calculation would be the adiabatic time-dependent Hartree-Fock theory,[16,17] in which a Hamiltonian in the space of elongation and necking coordinates, a reflection asymmetry coordinate, an axial asymmetry coordinate, and the conjugate momenta may be derived. Since the adiabatic hypothesis is well justified in this case and both the potential surface and corresponding mass parameters are completely defined in such a theory, one could in principle calculate a wave function yielding the probability distribution of all relevant configurations near the saddle point.

In induced fission, the most probable path corresponds to passing through the saddle point with negligible collective velocity. Thus, the obvious initial condition for our axial and reflection symmetric TDHF calculation is to use a static constrained HF solution calculated slightly beyond the saddle point. Although, in general, the shape of a constrained HF energy of deformation curve changes arbitrarily with the choice of constraining coordinate, the saddle point is unique. Since any infinitesimal push away from the saddle point yields the same path, requiring the initial quadrupole constrained configuration to be slightly beyond the saddle point (1 MeV below the maximum in our case) yields an essentially unique initial condition.

For a more general calculation in which one did not enforce symmetry and calculated an initial probability distribution for initial saddle configurations, an exactly symmetric initial condition is both extremely improbable and totally misleading (since it will not fission in the mean-field theory with no residual interaction). In contrast, all initial conditions with even infinitesimal symmetry breaking do fission. Thus the distribution of initial conditions is equivalent to a distribution of symmetry breaking matrix elements. So, very crudely, one could transform the distribution of initial conditions into a distribution of values for the effective pairing matrix element G or gap Δ. If the symmetry breaking matrix element were zero, G should just be the pairing strength $G \approx 23$ MeV$/A \approx 0.1$ MeV. For nonzero symmetry breaking, G should be correspondingly enhanced, and we shall subsequently investigate a reasonable range of possible G values.

C. Constant-gap pairing approximation

The equations of motion derived from applying the time-dependent variational principle to a BCS wave function with the assumption of a constant gap are very simple.[10] The single-particle wave functions evolve according to

$$i\dot{\phi}_l = (h - \epsilon_l)\phi_l, \tag{7}$$

where the single-particle Hamiltonian h obtained from variation of Eq. (1) is given in detail in Appendix I of Ref. 12 and the occupation probabilities in Eq. (4) are given by $\eta_l = v_l{}^2$. The u's and v's are determined by

$$i\frac{d}{dt}(v_l{}^2) = \Delta[(u_l v_l) - (u_l v_l)^*] \tag{8a}$$

and

$$i\frac{d}{dt}(u_l v_l) = 2u_l v_l(\epsilon_l - \lambda) + \Delta(2v_l{}^2 - 1), \tag{8b}$$

where

$$\epsilon_l = \int \phi_l^* h \phi_l \tag{9}$$

and the Lagrange multiplier λ is defined to conserve particle number:

$$\lambda = \left(\Delta N + \sum_{l>0}[\epsilon_l(u_l v_l + u_l v_l^*) - \Delta]\right) \Big/ \sum_{l>0}(u_l v_l + u_l v_l^*). \tag{10}$$

Since the constant gap theory is equivalent to a corresponding Landau-Zener energy-level crossing problem,[10] it is clear that in the early stages of fission during which the motion is very slow, the strength of Δ is immaterial. Once the collective velocity builds up, a large value of Δ will keep most of the probability in the lowest energy states, whereas a small value of Δ will greatly enhance the dissipation by causing non-negligible occupation of high-energy single-particle levels. Thus, there is an unavoidable interplay between the usual TDHF dissipation arising from the scattering of single-particle wave functions from the well edges and the dissipation originating from the Landau-Zener jump probabilities parametrized by Δ.

D. Computational methods

There are two principal approaches to the solution of the static HF equations and integration of the TDHF equations. In the familiar technique of expansion in a one- or two-center harmonic-oscillator (HO) basis,[18] matrix equations for the expansion coefficients are diagonalized or integrated in time for the static and dynamic problems, respectively. Although the oscillator expansion yields reasonably accurate variational bounds for static HF solutions, the accuracy is highly shape dependent, yielding energy of deformation curves

of uncertain and unquantifiable accuracy. In the alternative method of solution in coordinate space, the Hamiltonian is discretized on a rectangular mesh, replacing the functional of the individual single-particle wave functions by a function of the values of the single-particle wave functions on the mesh points. Because we have only been able to implement a 3-point second-difference formula in cylindrical coordinates,[11] the constrained HF energy is significantly less accurate than in the oscillator case and does not constitute a bound. However, as discussed below, the accuracy is quite independent of shape and thus offers significant advantages for problems like collisions and fission, where many different shapes are involved.

Solution in coordinate space

Matrix equations for the values of the single-particle wave functions at the mesh points are derived by varying a discretized Hamiltonian rather than discretizing the HF or TDHF differential equations. Hence, the resulting matrices are automatically Hermitian, and a well-defined approximation to the energy is exactly minimized in static HF and rigorously conserved in TDHF. The details of the static constrained HF calculation with the present interaction are presented in Ref. 12. The TDHF equations are solved by the Peaceman-Rachford method as described in Appendix A of Ref. 4 using the single-particle Hamiltonian matrix given in Ref. 12, modified to include the presence of a current.

As mentioned above, the primary inaccuracy in the energy arises from replacing derivatives by finite differences. Since the nuclear volume and interior potential remain essentially constant,[19] locally the nuclear wave function is approximately given by a Fermi sea of wave functions with maximum momentum k_F. At least on a rectangular mesh in Cartesian coordinates, one would then expect the discretization error to be independent of the nuclear shape. For this Cartesian case, the kinetic-energy error is easily estimated as follows. Since

$$-f''(x) \approx -\frac{f(x+\delta)+f(x-\delta)-2f(x)}{\delta^2}+\frac{\delta^2}{12}f''''(x), \quad (11)$$

the kinetic energy error per particle for a Fermi gas is

$$\frac{\hbar^2}{m}\frac{3}{280}k_F{}^4\delta^2, \quad (12)$$

corresponding to a fractional error of $\frac{1}{28}(k_F\delta)^2$.

For a mesh spacing δ of 1.0 fm, the largest used in this work, this estimate yields a 6% error or roughly 1.3 MeV per particle. The smallest mesh spacing used in this investigation, 0.65 fm, reduces the error to less than half this value. For the neutron to proton ratio in ^{236}U, this simple estimate yields an error in the total energy of 320 MeV for $\delta = 1.0$ fm and 135 MeV for $\delta = 0.65$ fm. The difference of 185 MeV is in fortuitously good agreement with the calculated HF energy difference of 200 MeV for the two meshes, given that we use cylindrical coordinates, have ignored discretization errors in the $\rho\tau$ term, and have omitted the Euler-Maclaurin corrections.[12] Thus, the fact that the kinetic energy is basically a volume contribution is one solid argument for the shape independence of the discretization error.

Additional evidence is provided by calculations of light nuclei in Ref. 12. The shape of the ^{58}Ni energy of deformation curve for $\delta = 0.55$ fm is extremely accurate, with the energy discrepancy being a shape-independent constant shift. Increasing the mesh spacing to $\delta = 1.1$ fm yields a curve of qualitatively similar shape, with the minima at approximately the same locations and comparable relative depth. The anisotropy of the mesh does not lead to significant orientation dependence, as shown by the near degeneracy of single-particle levels in the same j shell in ^{40}Ca, even on a 1.0 fm mesh. Also, the shape of the radial density distribution is not significantly altered by discretization on a finite mesh, as shown by the $\delta = 0.8$ fm results for ^{40}Ca. In that case, the density remains spherically symmetric, with only a small density compression resulting from the underestimate of the kinetic energy. (This and certain other gross effects of a 6% underestimate of the kinetic energy could be removed in subsequent investigations by defining an adjusted nucleon mass such that the total second-difference energy reproduces the proper total kinetic energy.) Since one might worry that discretization errors might contribute significantly to the surface energy, and thus produce a spurious deformation dependence, it is particularly reassuring that no serious discretization errors arise in the deformation energy of light nuclei we have discussed, where the ratio of surface to volume energy is much larger than in ^{236}U.

The final check on discretization errors is provided by selected comparisons of ^{236}U calculations on 1.0 and 0.65 fm meshes. The double humped fission barrier obtained with $\delta = 1.0$ fm shown subsequently in the lower right-hand frame of Fig. 1 is qualitatively unchanged by reduction of the mesh to 0.65 fm. The deformation at which the first minimum occurs is somewhat decreased, so for values of the quadrupole moment less than $1.5AR_0^2$, the 0.65 fm curve agrees somewhat more closely with the macroscopic-microscopic calculation in the lower left-hand frame of Fig. 2. Dynamic TDHF calculations with initial conditions con-

strained to have quadrupole moment $1.86AR_0^2$ were compared using a 16- by 40-point mesh with $\delta = 0.65$ fm and a 10- by 24-point mesh with $\delta = 1.0$ fm. The shapes of the resulting half-density contours differed negligibly at corresponding times. For example, for the case of $T = 3 \times 10^{-21}$ s shown in Fig. 6, the maximum discrepancy between half-density contours was less than 0.3 fm, which is at the limit of the uncertainty in interpolation and plotting. Prior to scission, elongation and deformation coordinates, as defined in Refs. 2 and 4, differed by less than 3% at corresponding times, and the maximum discrepancy in quadrupole moments was 6%. The final translational kinetic energy of the fission fragments was roughly 5 MeV lower for $\delta = 1.0$ fm than for $\delta = 0.65$ fm, although the $\delta = 0.65$ fm mesh was deliberately lengthened to obtain a more precise determination of this quantity.

On the basis of these arguments and numerical tests, we are confident that the discretization errors for the $\delta = 0.65$ fm mesh are under firm control and should not affect any of the conclusions of this work. Indeed, given the fact that the $\delta = 0.65$ fm fission calculation requires 30 minutes of CDC 7600 time, additional numerical accuracy does not appear commensurate with the serious physical approximation of constant-gap pairing and the omission of the spin-orbit force.

Truncation of pairing space

Solution, either on a mesh or by an oscillator expansion,[20] requires truncation of the space of unoccupied single-particle orbitals. In coordinate space, it is convenient to truncate at the onset of the continuum and thus remove explicit dependence on the volume enclosed by the mesh boundaries. This truncation yields roughly 100 active single-particle wave functions of which 20 are normally unoccupied. In each angular momentum projection and parity subspace, there is at least one unoccupied orbital, so the most crucial level crossings should always be included. For a given gap Δ, the strength of the pairing matrix element G depends on the truncation of the pairing space. The constant gap pairing energy $\tilde{E}$ is twice the true pairing energy and may be written

$$\tilde{E} = -2G \sum_{l>0} [\eta_l(1-\eta_l)]^{1/2} = -2(\Delta^2/G) . \qquad (13)$$

For our calculation, truncating the pairing space at the continuum yields $G = 0.12$, 0.17, and 0.29 MeV for $\Delta = 0.7$, 2.0, and 6 MeV, respectively. Since 23 MeV/A gives 0.1 MeV and realistic matrix elements in the uranium region[21] average 0.15 MeV, and range from 0.0 to 0.4 MeV, it is clear that the lower values of Δ correspond roughly to the strength of the true residual interaction. The highest value effectively accounts for the additional strength of symmetry breaking matrix elements.

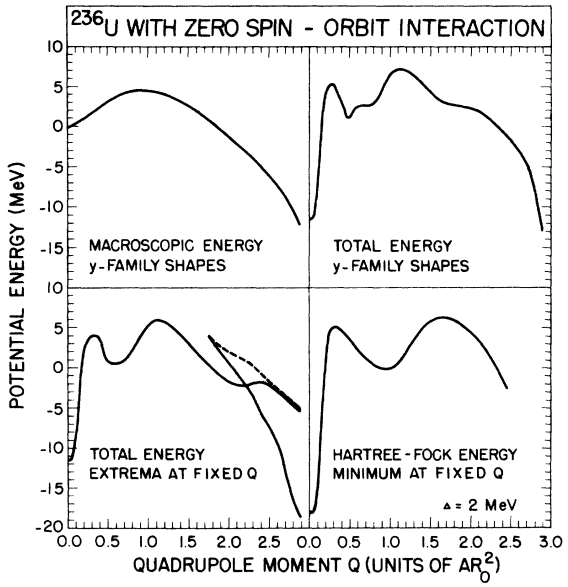

FIG. 1. Potential energy of ^{236}U with zero spin-orbit interaction vs matter quadrupole moment Q.

In an oscillator expansion, it is straightforward to include unbound states which provide a discrete approximation to the continuum. In principle, these states are just as arbitrary as continuum states normalized in a box, but are somewhat more convenient because they are localized in the region of the nucleus. The effect of different truncations of

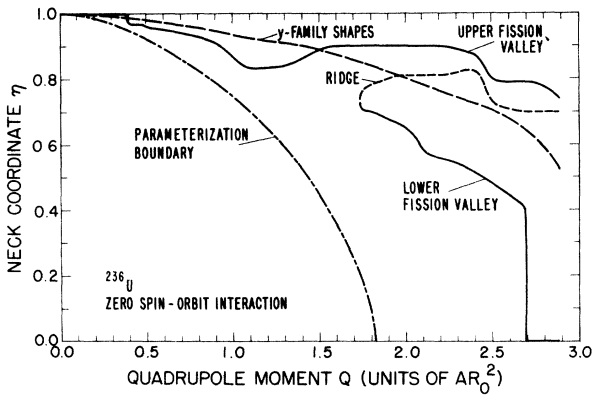

FIG. 2. Locations in the Q-η plane of our parametrization boundary, y-family shapes, and valleys and ridge in the macroscopic-microscopic potential-energy surface of ^{236}U with zero spin-orbit interaction. The neck coordinate η is defined as the ratio of the neck radius of the shape to the neck radius of a spheroid with the same quadrupole moment.

the continuum are being explored in a two centered HO basis by Flocard.[20]

III. MACROSCOPIC APPROACH

In a macroscopic hydrodynamical description of large-scale nuclear collective motion, one starts with a distribution of matter that is subjected to given forces and solves the resulting classical equations of motion in some approximation. Although attempts have been made recently to solve the equations of motion directly by use of finite-difference techniques,[22-24] the more common procedure is to assume that the matter is incompressible and to parametrize the nuclear shape in some way, which leads to a system of coupled nonlinear differential equations that is in turn solved numerically.[14,15,25-36] This latter method is relatively simple, concentrates on a few essential degrees of freedom, and permits incorporating microscopic effects into an otherwise macroscopic model. In such an approach one first specifies the degrees of freedom by parametrizing the nuclear shape, and then specifies three fundamental quantities: (1) the nuclear potential energy of deformation, (2) the collective kinetic energy, and (3) the dissipation mechanism for converting collective energy into internal single-particle excitation energy.

A. Degrees of freedom

We restrict ourselves to axially symmetric nuclei and describe the shape of a fissioning nucleus prior to scission in terms of smoothly joined portions of three quadratic surfaces of revolution.[14,15,29-36] The results reported here are also restricted to reflection-symmetric nuclei, which means that we consider explicitly only three degrees of freedom. These specify the distance between the two end spheroids that form the shape, the eccentricity of these end spheroids, and the eccentricity of the middle quadratic surface that forms the neck.

After scission, which occurs when the repulsive Coulomb force overcomes the attractive nuclear force and ruptures the neck,[35] the fission fragments are described in terms of two separated spheroids.[14,31,35] The transition from one shape parametrization to the other is accomplished by equating the two most important central moments of the matter distribution and their time derivatives before and after scission.[31,35] This introduces a small but nevertheless tolerable discontinuity in the various contributions to the total energy. Throughout our discussion we use the notation

$$q = q_1, q_2, \ldots, q_N$$

for the N generalized coordinates that specify the nuclear shape.

B. Potential energy of deformation

We calculate the nuclear potential energy of deformation $V(q)$ by means of a macroscopic-microscopic approach,[37-39] with the smooth trends of the potential energy obtained from a modified liquid-drop model[40-43] and the local fluctuations obtained by means of Strutinsky's method[44,45] from a folded Yukawa single-particle model.[36] In the dynamical calculations themselves, we neglect the single-particle corrections, but they are nevertheless useful for comparing with the static constrained HF potential-energy surface.

The modified liquid-drop model includes the repulsive Coulomb energy and the attractive nuclear macroscopic energy. The Coulomb energy of a deformed nuclear system is calculated for a uniformly charged, sharp-surface body according to Eq. (2), with an interior proton density

$$\rho_p = Z/(\tfrac{4}{3}\pi R_0^3).$$

The radius of the spherical nucleus is given by

$$R_0 = r_0 A^{1/3},$$

where r_0 is the nuclear-radius constant. The integrations are over the volume of the deformed system; as the system deforms, this volume is assumed to remain constant at $\frac{4}{3}\pi R_0^3$. Because the first-order surface-diffuseness correction to the Coulomb energy is zero, the second-order correction is independent of shape,[47] and the third-order correction is proportional to the surface area,[48] this method takes into account implicitly the effect of the surface diffuseness on the Coulomb energy through third order in diffuseness.

In analogy with the calculation of the Coulomb energy, the nuclear macroscopic energy is calculated by means of a double integral of a Yukawa two-body interaction potential over the volume of the deformed system.[40-43] In particular,

$$E_{nm} = -\frac{c_s}{8\pi^2 a^3 r_0^2 \rho_q^2} E_Y, \tag{14}$$

where E_Y is given in Eq. (3) and the strength is defined to reproduce the proper surface energy. The quantity r_0 is as before the nuclear-radius constant, $a = 1/\mu$ is the range of the Yukawa potential, and $\rho_q = A/(\frac{4}{3}\pi R_0^3)$ is here the interior nucleon density. Furthermore,

$$c_s = a_s\left[1 - \kappa\left(\frac{N-Z}{A}\right)^2\right], \tag{15}$$

where a_s is the surface-energy constant and κ is

the surface-asymmetry constant. The values of these constants are[40-43]

$$r_0 = 1.16 \text{ fm},$$
$$a = 1.4 \text{ fm}, \quad (16)$$
$$a_s = 24.7 \text{ MeV},$$

and

$$\kappa = 4.0.$$

To lowest order in the Yukawa range, this method for calculating the nuclear macroscopic energy yields the surface energy of the liquid-drop model. The higher-order corrections are associated with the finite range of the nuclear force and lower the energy relative to the surface energy. These finite-range corrections are very important for certain shapes, such as those near the scission point in fission and those near the point of first contact in heavy-ion reactions.

The microscopic shell and pairing corrections are calculated by means of Strutinsky's method[44,45] applied to the single-particle levels obtained from a folded Yukawa potential.[46] This is a diffuse-surface single-particle potential generated by folding a Yukawa function over a finite square-well potential of the appropriate geometrical shape. In order to compare with the static constrained HF potential-energy surface, we set the spin-orbit interaction strengths λ_n and λ_p for neutrons and protons equal to zero. The remaining parameters V_n, V_p, R_0, and a, which define the depths of the neutron and proton single-particle potentials, their overall size, and their surface diffuseness, are taken from Refs. 49 and 50. The Coulomb potential for protons is calculated by assuming that the protons are distributed uniformly over the same shape and volume as the square well that generated the single-particle potential. Once the single-particle levels are known, the shell and pairing corrections are calculated by means of the procedures discussed in Ref. 46.

C. Collective kinetic energy

We calculate the collective kinetic energy for incompressible, nearly irrotational hydrodynamical flow. Because the collective velocities are small compared to the nuclear sound speed, the restriction to incompressible flow should be adequate. On the other hand, the collective velocities are sufficiently large that the adiabatic cranking approximation[51] for computing the collective kinetic energy is not valid. Because of the moderate collective velocities and because the pairing residual interaction is effectively destroyed at the high excitation energies that are present, there are no large transfers of matter at level crossings, which suggests that the collective kinetic energy is approximately that for irrotational collective-shape flow.[52] As an approximation to irrotational flow we use the Werner-Wheeler method, which determines the flow in terms of circular layers of fluid.[14,15,29-36]

With this approximation, the collective kinetic energy depends quadratically on the generalized velocities, i.e.,

$$T = \frac{1}{2} \sum_{i,j} M_{ij}(q) \dot{q}_i \dot{q}_j, \quad (17)$$

where time differentiation is denoted by a dot. The shape dependence of T is contained in the elements $M_{ij}(q)$ of the inertia tensor, the calculation of which is discussed in Refs. 15 and 31.

D. Dissipation mechanisms

We study three different mechanisms for the conversion of collective energy into internal single-particle excitation energy: ordinary two-body viscosity,[31,32,35] original one-body dissipation,[32,35,53-56] and modified one-body dissipation.[36] In each case, the Rayleigh dissipation function may be written in the quadratic form

$$F = \frac{1}{2} \sum_{i,j} \eta_{ij}(q) \dot{q}_i \dot{q}_j, \quad (18)$$

where $\eta_{ij}(q)$ denotes an element of the shape-dependent damping tensor. The rate of dissipation of collective energy into internal energy is equal to $2F$.

For an incompressible fluid with a constant two-body viscosity coefficient μ, the Rayleigh dissipation function is given by the volume integral[31,58]

$$F_{\text{2-body}} = \tfrac{1}{2}\mu \int \{\nabla^2 v^2 + (\vec{\nabla}\times\vec{v})^2 - 2\vec{\nabla}\cdot[\vec{v}\times(\vec{\nabla}\times\vec{v})]\}\, d^3r, \quad (19)$$

where $\vec{v}$ is the velocity of the fluid inside the shape. For irrotational flow the last two terms of this expression are zero, and the Gaussian divergence theorem may be used to transform the first term into the surface integral

$$F^{\text{ir}}_{\text{2-body}} = \tfrac{1}{2}\mu \oint (\vec{\nabla} v^2)\cdot d\vec{S}, \quad (20)$$

where $d\vec{S}$ denotes an outward-directed element of surface area. However, in the Werner-Wheeler approximation that we use, the flow contains a small rotational component. Formulas for the evaluation of F using the complete expression are given in Ref. 31.

Ordinary two-body viscosity, which arises from collisions between individual nucleons, damps

multipole oscillations of high-degree more rapidly than those of low degree. In fission, two-body viscosity leads to more elongated scission shapes and to decreased fission-fragment kinetic energies compared to the nonviscous case. Experimental most probable fission-fragment kinetic energies for the fission of nuclei throughout the Periodic Table are reproduced adequately by a two-body viscosity coefficient of

$$\mu = 0.03 \pm 0.01 \text{ TP}$$
$$= 19 \pm 6 \times 10^{-24} \text{ MeV s/fm}^3, \quad (21)$$

when account is taken of the rupture of the neck at a finite radius.[35]

Two-body dissipation is physically suspect because, due to the Pauli exclusion principle, the collision mean free path of a nucleon inside a nucleus is larger than the nuclear diameter. Thus, it is interesting to consider an alternative approximation in which the nucleus does not dissipate collective energy through collisions between individual nucleons, but instead through nucleons colliding with the moving boundary of the nucleus.[32,35,53-57] Clearly, this approximation is much closer in spirit to that of TDHF. In the original derivation of this one-body dissipation, the Rayleigh dissipation function is given by the surface integral[55-57]

$$F_{\text{1-body}} = \tfrac{1}{2}\rho\bar{v}\int v_n^2 dS, \quad (22)$$

where ρ is the mass density, $\bar{v}$ is the average speed of the nucleons inside the nucleus, and v_n is the normal velocity of the surface. For a Fermi-gas model of the nucleus, $\bar{v}$ is equal to $\frac{3}{4}$ the Fermi velocity. In the derivation of this expression it is assumed that $|v_n| \ll v_F$ and that there is no overall motion of the matter inside the nucleus.

This original formula for one-body dissipation predicts that nuclei should be highly dissipative and—unlike the case for ordinary two-body viscosity—that multipole oscillations of low degree should be damped more rapidly than those of high degree. In fission this leads to a slow descent from saddle to scission and to a compact scission configuration. With no adjustable parameters used, the resulting calculated most probable fission-fragment kinetic energies for the fission of nuclei throughout the Periodic Table are in approximate agreement with experimental values. In particular, the calculated energies are about 8% larger than the experimental values, when account is taken of the rupture of the neck at a finite radius.[35]

In dynamical calculations of fission, the original formula for one-body dissipation is suspect in the later stages of fission because for the uniform translation of the fission fragments it yields a finite dissipation rather than zero. For either a uniform translation or a uniform rotation, the original formula may be modified to remove this spurious dissipation, but there is no satisfactory way to interpolate between the one-body dissipation formula that applies to compact shapes and that which applies to shapes with separating end bodies.

An attempt has been made to modify the formula for one-body dissipation by incorporating self-consistency in a heuristic way.[36] In this modification, the normal velocity v_n is replaced by the relative normal velocity Δv_n between the nuclear surface and the matter colliding with it. This relative normal velocity is approximated by the first term in a Taylor-series expansion of $\vec{v}$ about a point on the surface, which leads to

$$\Delta v_n = \lambda \hat{n} \cdot \frac{\partial \vec{v}}{\partial n} + \cdots .$$

The range λ is the effective distance between the nuclear surface and the matter colliding with it, $\hat{n}$ is the outward-directed normal unit vector at the surface, and the normal derivative $\partial/\partial n = \hat{n} \cdot \vec{\nabla}$ is evaluated at the surface. With this replacement, the modified formula for one-body dissipation becomes[36]

$$F_{\text{1-body}}^{\text{mod}} = \tfrac{1}{2}\rho\bar{v}\lambda^2 \oint \left(\hat{n} \cdot \frac{\partial \vec{v}}{\partial n}\right)^2 dS. \quad (23)$$

This modified formula leads automatically to zero dissipation for either a uniform translation or a uniform rotation, as should be the case.

The properties of modified one-body dissipation are qualitatively similar to those of ordinary two-body viscosity rather than to those of the original one-body dissipation. In particular, it damps multipole oscillations of high degree more rapidly than those of low degree, and in fission it leads to more elongated scission shapes and to decreased fission-fragment kinetic energies. Experimental most probable fission-fragment kinetic energies for the fission of nuclei throughout the Periodic Table are reproduced adequately by the value

$$\lambda^2 = 3 \pm 1 \text{ fm}^2, \quad (24)$$

when account is taken of the rupture of the neck at a finite radius.[36]

E. Equations of motion

We determine the time evolution of the system by solving numerically classical equations of motion. The classical approximation is valid as long as the de Broglie wavelength for motion in a given direction is small compared to the distance over which the potential changes appreciably. Except for motion close to the saddle point, this condition

is in general satisfied in fission.

The generalized Lagrange equations of motion are[31,38,59]

$$\frac{d}{dt}\left(\frac{\partial L}{\partial \dot{q}_i}\right)-\frac{\partial L}{\partial q_i}=\frac{\partial F}{\partial \dot{q}_i}, \quad i=1,2,\ldots,N, \tag{25}$$

where

$$L(q,\dot{q})=T(q,\dot{q})-V(q) \tag{26}$$

is the Lagrangian for the system. Upon substituting Eqs. (17), (18), and (26) into Eq. (25) and using the symmetry of the inertia and damping tensors, we obtain

$$\sum_j M_{ij}(q)\ddot{q}_j+\sum_{j,k}\left[\frac{\partial M_{ij}(q)}{\partial q_k}-\frac{1}{2}\frac{\partial M_{jk}(q)}{\partial q_i}\right]\dot{q}_j\dot{q}_k$$

$$+\sum_j \eta_{ij}(q)\dot{q}_j+\frac{\partial V(q)}{\partial q_i}=0, \quad i=1,2,\ldots,N, \tag{27}$$

a system of N coupled nonlinear differential equations for the generalized coordinates.

We find it convenient in practice to transform these equations into the generalized Hamilton equations of motion, which are a system of $2N$ coupled nonlinear first-order differential equations for the generalized coordinates and generalized momenta.[31] Then, for a given set of initial conditions, we integrate these equations numerically by use of a fourth-order Adams-Moulton predictor-corrector method,[60] with the starting procedure based on a modified fourth-order Runge-Kutta method.[60,61]

IV. CALCULATED POTENTIAL ENERGY

As an aid in interpreting the results of the dynamical calculations to be presented in Sec. V, we now compare the static potential energy calculated in various ways for a ^{236}U nucleus without spin-orbit interaction. Because for the macroscopic energy and the macroscopic-microscopic energy we have calculated two-dimensional potential-energy surfaces as functions of the quadrupole moment and a neck coordinate, we discuss these energies first. This is followed by a discussion of the constrained HF energy as a function of the quadrupole moment.

A. Macroscopic energy

As discussed in Sec. IIIA, our three-quadratic-surface shape parametrization contains three symmetric degrees of freedom. For displaying the calculated potential energy, it is useful to project out of this three-dimensional space the most important deformation leading to fission. Although the precise determination of the fission coordinate would require performing a dynamical calculation, during the early stages of fission the y-family shapes introduced by Hill and Wheeler provide a fair approximation to the fission coordinate.[46,62] These shapes correspond to the saddle-point shapes for a uniformly charged liquid drop and range from a single sphere through symmetric dumbbell-like shapes to two tangent spheres. The advantage of the y-family shapes over other one-parameter families is that they include automatically the liquid-drop-model saddle-point shapes for all nuclei, which are fairly close to the actual saddle-point shapes of interest.

In the upper left-hand portion of Fig. 1 we show the macroscopic energy of ^{236}U calculated along the y-family shapes. For ease of later comparisons the energy is plotted versus the matter quadrupole moment Q, in units of AR_0^2, where A is the mass number and R_0 is the radius of the equivalent sharp-surface spherical shape. With increasing deformation from the spherical shape, the macroscopic energy increases monotonically until it reaches a maximum value of 4.5 MeV and then decreases monotonically.

To explore the effect on the potential energy of an additional degree of freedom, we now introduce a neck coordinate η (not to be confused with the elements of the damping tensor denoted by the same symbol). This coordinate is defined as the ratio of the neck radius of the shape to the neck radius of a spheroid with the same quadrupole moment. In order to generate a two-parameter family of shapes as a function of Q and η, we must eliminate the third degree of freedom appearing in the symmetric three-quadratic-surface space parametrization. This we do by requiring that for a given value of Q the eccentricity of the two end spheroids comprising the shape remain equal to that for the corresponding y-family shape.

For small values of Q there is a minimum value of η below which we are unable to generate a shape in the three-quadratic-surface parametrization. The lower boundary of shapes accessible in this parametrization is shown by the dot-dashed curve in Fig. 2. The y-family shapes lie along the long-dashed curve, and the top of the figure at $\eta=1$ corresponds to pure spheroidal distortions.

We show in Fig. 3 the macroscopic energy for ^{236}U as a function of Q and η. The position of the saddle point is located approximately along the y-family shapes. Also, for values of $Q/AR_0^2 \leq 2.5$ the static fission valley (defined here as the position of the minimum energy with respect to η for a fixed value of Q) lies fairly close to the y-family shapes. For larger values of Q the fission valley disappears, and the minimum energy is located instead in the fusion valley corresponding to two separated nuclei.[42]

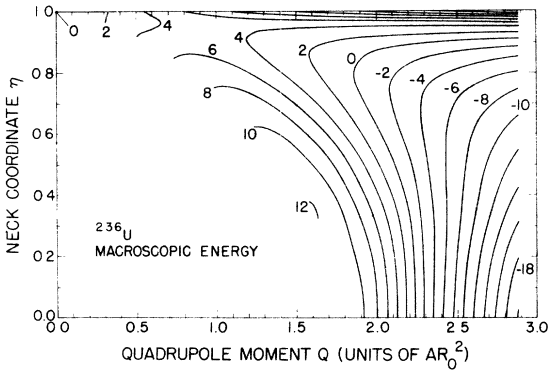

FIG. 3. Contours in the Q-η plane of the macroscopic potential energy of ^{236}U, in units of MeV.

B. Macroscopic-microscopic energy

For y-family deformations, the effect of adding microscopic shell and pairing corrections to the macroscopic energy is shown in the upper right-hand corner of Fig. 1. For zero spin-orbit interaction, the energy of ^{236}U is lowered at the spherical shape by 11.6 MeV relative to the macroscopic energy. The fission barrier contains two prominent peaks plus a small plateau located near the second minimum. With 0.5 MeV of zero-point energy taken into account at the ground state, the calculated fission-barrier height is 18.2 MeV, which is substantially larger than the experimental value[63] of 5.7 ± 0.2 MeV. The large calculated value arises primarily because of the neglect of the spin-orbit interaction, but also partly because of the neglect of mass-asymmetric deformations. For the two-dimensional space of quadrupole moment Q and neck coordinate η, the effect of adding microscopic shell and pairing corrections to the macroscopic energy is shown in Fig. 4. Between the sphere and the vicinity of the second saddle point, the two-dimensional potential-energy surface is qualitatively as anticipated on the basis of the results for the y-family shapes. In particular, the increased binding at the spherical shape, plus the existence of the first saddle point, the second minimum, and the second saddle point may be seen in the two-dimensional surface.

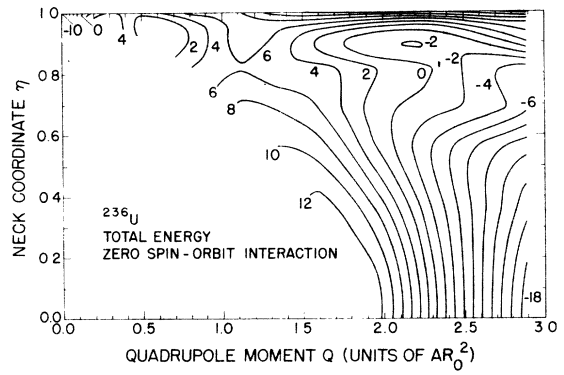

FIG. 4. Contours in the Q-η plane of the macroscopic-microscopic potential energy of ^{236}U with zero spin-orbit interaction, in units of MeV.

However, beyond the vicinity of the second saddle point the microscopic shell and pairing corrections separate the fission valley into two distinct valleys with a ridge between them. The energy in the lower fission valley decreases monotonically, whereas the upper fission valley contains a small third minimum followed by a small third saddle point. The lower fission valley disappears at $Q/AR_0^2 \approx 2.7$, and the upper fission valley presumably disappears at a point slightly outside the region where the energy is calculated. For larger deformations the minimum energy is located in the fusion valley corresponding to two separated nuclei.[42]

The locations of the fission valleys in the Q-η space are shown by the solid curves in Fig. 2, and the location of the ridge between them is shown by the short-dashed line. For small deformations the fission valley corresponds to pure spheroidal deformations, whereas at $Q/AR_0^2 \approx 0.4$ it shifts to shapes with smaller neck radii than those of y-family shapes. At $Q/AR_0^2 \approx 1.5$ the valley shifts back to shapes with larger neck radii than those of y-family shapes. Beyond $Q/AR_0^2 \approx 1.7$ the two fission valleys are located on opposite sides of the y-family shapes. For these large deformations the y-family shapes are actually fairly close to the potential-energy ridge between the two fission valleys.

The potential energy along the valleys is shown by the solid lines in the lower left-hand corner of Fig. 1, and the potential energy along the ridge is shown by the short-dashed curve. Apart from the presence of two valleys for $Q/AR_0^2 \gtrsim 1.7$, this curve is qualitatively similar to the result for y-family shapes shown in the upper right-hand portion of the figure. However, the small plateau near the second minimum has now disappeared, and the energy has decreased slightly for most deformations. For example, the calculated fission-barrier height is now 17.0 MeV, which is a reduction of 1.2 MeV.

C. Constrained Hartree-Fock energy

At first sight the constrained HF energy as a function of Q, shown in the lower right-hand portion of Fig. 1 for an effective gap Δ of 2.0 MeV and a grid spacing of 1.0 fm, looks very different from the macroscopic-microscopic result in the upper right hand section of the same figure. This apparent discrepancy and the need to understand the

constrained HF solutions in detail motivated the thorough investigation of the macroscopic-microscopic energy-of-deformation surface described in Sec. IV B.

The discovery of two fission valleys and the calculation of the energy minimum with respect to η at fixed Q essentially resolve the apparent discrepancies between the two methods, and give useful insight into several puzzling aspects of the constrained HF problem. The subsidiary plateau at $Q \approx 0.6\text{–}0.8AR_0^2$ for the y-family shapes is removed when the energy is minimized with respect to η, yielding qualitative agreement with the HF curve at low Q. The double-valued behavior beyond $Q = 1.8AR_0^2$ in the lower left-hand portion of Fig. 1 is also consistent with the HF results if one assumes that the HF solutions correspond to the local minima in the lower fission valley.

Since a HF calculation with a single constraint has no control over which local minimum is attained, it is not surprising that the present coordinate space solutions and similar two-center HO calculations[20] sometimes yielded large-Q solutions with qualitatively different degrees of necking. The coordinate-space density contours are compared with the minimum-energy macroscopic-microscopic shapes at representative values of Q in Fig. 5. Here, one clearly observes that at $Q = 1.86AR_0^2$ the HF solution corresponds to the lower fission valley configuration. Thus, the high-Q HF results in the lower right-hand portion of Fig. 1 really should be compared with the lower valley segment in the lower left-hand portion of Fig. 1. Since the constrained HF wave functions at a given Q were generated iteratively from a previous solution at slightly lower Q, and because the shapes varied smoothly and regularly with Q, we are confident that all other high-Q solutions also correspond to the lower valley. A crude attempt to generate solutions in the upper valley using both quadrupole and hexadecapole constraints failed, presumably because a hexadecapole field of sufficient strength to eliminate the neck significantly disrupts the end caps.

Having achieved qualitative agreement between the macroscopic-microscopic and HF results, several quantitative comments are relevant. As noted in Sec. IID, decreasing the mesh spacing from 1.0 to 0.65 fm brought the position and width of the second HF minimum into excellent agreement with the lower left-hand portion of Fig. 1. The HF fission barrier height is sensitive to the pairing strength, as expected from Strutinsky's arguments, ranging from 20 MeV for $\Delta = 6$ MeV to 32 MeV for $\Delta = 0.7$ MeV. Presumably the difference between the HF and macroscopic barrier heights arises from somewhat different level spacings in the two single-particle potentials.

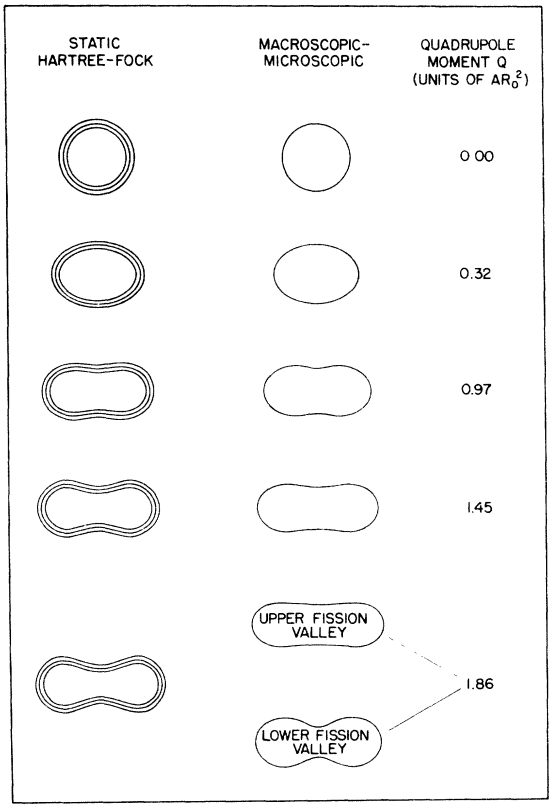

FIG. 5. Comparison as a function of quadrupole moment of shapes for ^{236}U with zero spin-orbit interaction calculated in the static constrained-Hartree-Fock approximation and in the macroscopic-microscopic method. In the former case, the contours correspond to matter densities of 0.02, 0.08, and 0.14 nucleons/fm^3, which represent approximately $\frac{1}{8}$, $\frac{1}{2}$, and $\frac{7}{8}$ of the density of nuclear matter.

Although we believe the constrained HF solutions are understood adequately for our present purposes, the elucidation of the topology of the multidimensional static HF potential energy surface remains an important challenge for the future.

D. Specification of initial conditions

As discussed in Sec. IIB, when a nucleus undergoing induced fission passes through the vicinity of its saddle point, the probability that a particular normal coordinate or momentum has a specified value is to lowest order a Gaussian distribution. The most probable initial conditions for induced fission therefore correspond to starting from rest at the fission saddle point. Because classically it would require an infinite time for fission to occur from such an unstable equilibrium point, it is nec-

essary in practice either to give the system a small amount of initial kinetic energy directed toward fission or to start it a short distance beyond the fission saddle point.

For both the macroscopic and microscopic calculations, we have started the system from rest at a point with energy 1 MeV below that of the corresponding saddle point. For the macroscopic calculations, this point is chosen along the most probable path for nonviscous flow, which is determined by starting the system from rest an infinitesimal distance in the fission direction beyond the saddle point. For the microscopic calculations, this point is chosen along the static constrained-HF curve for $\Delta = 2$ MeV. The initial shape for the microscopic calculation lies in the lower fission valley of the total potential-energy surface. It is more deformed than the initial shape for the macroscopic calculation, which would be expected at first sight to make the comparison between the two dynamical calculations difficult.

However, for dissipative systems, the later stages of the dynamical evolution, as well as such calculated quantities as the final fission-fragment kinetic energies of the fragments at infinity, are surprisingly insensitive to the initial conditions that are used. To check this sensitivity, we also used for the macroscopic calculations an initial shape that was constructed to reproduce optimally the initial microscopic shape. With the exception of the nonviscous case, the final results were similar to those obtained with the original initial conditions. For the microscopic calculations, we also used initial conditions corresponding to starting from rest 6 MeV beyond the saddle point. The final results differed negligibly from those obtained with the original initial conditions.

V. RESULTS OF DYNAMICAL CALCULATIONS

The results of the microscopic and macroscopic calculation for the fission of ^{236}U are summarized in Figs. 6 and 7 and Tables II and III.

A. TDHF solutions

Density contours for a TDHF fission calculation with a gap of 2 MeV are shown in the left-hand column of Fig. 6 at intervals of 10^{-21} s. The three contours denote $\rho = 0.02$, 0.08, and 0.14 fm^{-3}, corresponding to roughly $\frac{1}{8}$, $\frac{1}{2}$, and $\frac{7}{8}$ of nuclear matter density, respectively. The middle contour is therefore most directly comparable to the sur-

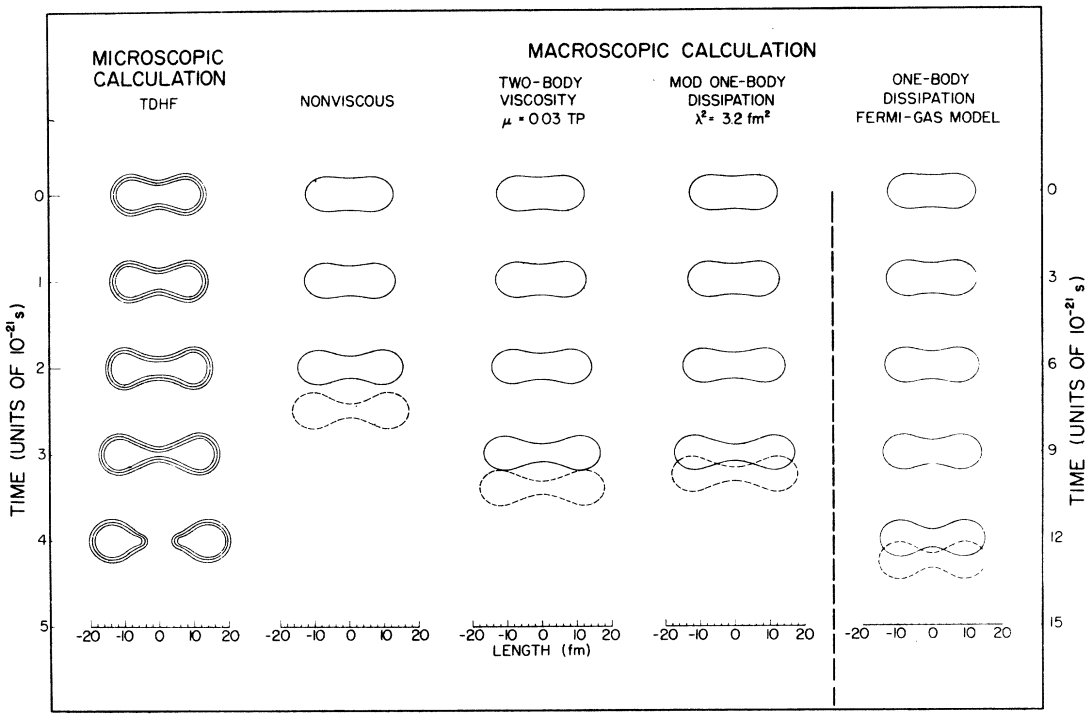

FIG. 6. Comparison as a function of time of shapes for ^{236}U with zero spin-orbit interaction calculated in the TDHF approximation for $\Delta = 2$ MeV and in a macroscopic approach with various types of dissipation. For modified one-body dissipation, we show the result for the preliminary value of $\lambda^2 = 3.2$ fm^2; the final value is 3 fm^2 (Ref. 36). Note that the time scale for the original one-body dissipation is 3 times as long as the time scale for the remaining cases.

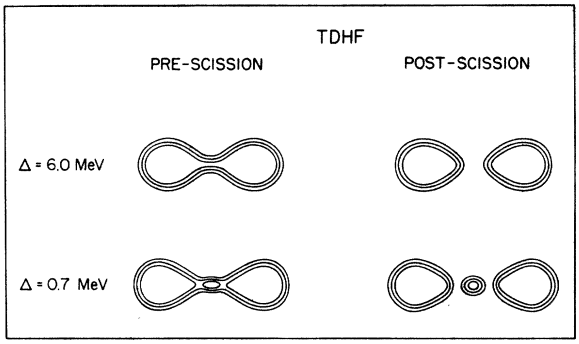

FIG. 7. Comparison of prescission and postscission shapes for ^{236}U with zero spin-orbit interaction calculated in the TDHF approximation for two values of the effective pairing gap Δ. The elapsed time between the two configurations for each Δ is 0.4×10^{-21} s.

face in a macroscopic calculation. In order to avoid confusion, the interior density fluctuations have been suppressed in this figure, but may be observed in Fig. 1 of Ref. 19. The solution at time $T=0$ is the initial constrained HF wave function with $Q=1.86AR_0^2$. As discussed previously, this configuration corresponds to a deformation 1 MeV below the barrier in the second fission valley and, because of shell effects, has a smaller neck radius than the macroscopic y-family shape in the remaining columns.

The time evolution of the density is completely consistent with one's intuitive expectations. As indicated by the $\frac{1}{8}$ and $\frac{7}{8}$ density contours, the surface comprises a sizable fraction of the nucleus and remains very accurately constant in thickness. Elongation and neck formation involve gradual shape deformation of the entire nucleus, and scission is a very smooth, continuous process due to the finite surface thickness and exponential fall off of single-particle orbitals. The last remnant of the neck, which shows up as the sharp bulges in the receding fission fragments of course quickly disappear during subsequent evolution of the system. The time scale is fast, with scission occurring within 3.4×10^{-21} s, in contrast to the much slower one-body dissipation theory to be discussed subsequently.

The dependence of the dynamics on the value of the gap is shown in Fig. 7 and Table II. The prescission and postscission shapes for $\Delta=6$ MeV in Fig. 7 are qualitatively similar to those in Fig. 6 for a 2 MeV gap. In detail, the interior density is slightly smoother, as expected for very strong pairing. The case of a 0.7 MeV gap, however, is quite different with an α-like cluster remaining in the neck region. The mean diameter of the half-density contour is roughly 3.5 fm, in excellent agreement with the value of 3.7 fm expected for an α particle.

Whereas the ternary fission may be partially fortuitous, it is highly suggestive of the known emission of α particles from the neck region with a probability of 1 in 600. That matter should get trapped in the neck region in the small gap limit, if at all, follows from the fact that small coupling matrix elements yield non-negligible occupation of the higher-energy orbitals localized in the neck. Furthermore, if we consider an ensemble of values of Δ, corresponding to a wave packet of symmetry-violating initial conditions, only those very

TABLE II. Comparison of calculated properties at the point of neck rupture for the fission of the compound nucleus ^{236}U. The initial conditions correspond in each case to starting from rest 1 MeV beyond the fission saddle point.

Result	Time (10^{-21} s)	Translational kinetic energy (MeV)	Vibrational kinetic energy (MeV)	Dissipated energy (MeV)	Potential energy (MeV)
		Microscopic			
$\Delta=6.0$ MeV	2.2	11	...	...	...
$\Delta=2.0$ MeV	3.4	12	...	...	...
$\Delta=0.7$ MeV	5.0	...	...	...	...
		Macroscopic			
Nonviscous	2.5	24.1	1.7	0.0	−22.4
Two-body viscosity, $\mu=0.03$ TP	3.4	18.1	0.6	11.9	−27.1
Modified one-body dissipation, $\lambda^2=3$ fm^2	3.2	18.2	0.6	11.9	−27.3
One-body dissipation, Fermi-gas value	12.9	0.5	0.1	17.6	−14.7

TABLE III. Comparison of experimental and calculated most probable fission-fragment kinetic energies for the fission of the compound nucleus ^{236}U. The initial conditions for each calculation correspond to starting from rest 1 MeV beyond the fission saddle point.

Result	Kinetic energy (MeV)
Experimental[a]	168.0±4.5
Microscopic	
$\Delta=6$ MeV	166
$\Delta=2$ MeV	142
Macroscopic	
Nonviscous	186
Two-body viscosity, $\mu=0.03$ TP	167
Modified one-body dissipation, $\lambda^2=3$ fm^2	166
One-body dissipation, Fermi-gas value	177

[a] For the fission of ^{232}Th induced by 65.0 MeV α particles, averaged over all fission-fragment mass divisions and corrected for the effects of fragment neutron emission (Ref. 64).

rare initial conditions which have negligible asymmetry can yield a total effective matrix element as small as the realistic pairing $G=0.12$ MeV corresponding to $\Delta=0.7$ MeV. Increasing G beyond this value yields two-body states in our calculations, so it is plausible that TDHF is even consis tent with the relative rarity of such events.

One possible measure of the translational kinetic energy at the point of neck rupture is given by $\frac{1}{2}$ the reduced mass of the system times $\dot{r}^2$ at that point, where $\dot{r}$ is the time derivative of the distance r between the centers of mass of the two halves of the system. The scission time, this translational kinetic energy, and the Coulomb energy at scission are tabulated in Table II for various values of Δ, although there is some arbitrariness in the definition of the point of neck rupture for the smooth scission occurring in TDHF. The asymptotic translational kinetic energies of binary fission fragments are tabulated and compared with experiment in Table III. The experimental result shown in Table III corresponds to the fission of ^{232}Th induced by 65.0 MeV α particles.[64] This reaction was selected because at this excitation energy the most probable fission-fragment mass division is into two equal fragments and the most probable fission-fragment kinetic energy is relatively insensitive to excitation energy, which suggests that single-particle effects have become negligible. The result corresponds to a weighted average over all mass divisions and has been corrected for the effects of neutron emission from the fragments. In accordance with usual practice, we refer loosely to this result as the most probable fission-fragment kinetic energy.

As observed in Table III, the fission fragment translational kinetic energy increases with increasing effective gap. This is consistent with the fact that less probability is retained in highly excited states for large Δ, and is usually described in terms of dissipation. Since ternary events were not envisioned when the calculation of asymptotic translational energies was programed, we have no result for the case of the 0.7 MeV gap.

The 20 MeV change in asymptotic kinetic energy between $\Delta=6$ MeV and $\Delta=2$ MeV is interesting and has several important implications. First, it is evident that we cannot use fission as a definitive test of dissipation in the mean-field theory until we obtain an accurate theoretical calculation of Δ or include asymmetry. Second, compared with 20 MeV, the various uncertainties in the calculation of final kinetic energies are inconsequential. The 5 MeV uncertainty associated with the mesh size has already been discussed. With total constant-gap pairing energies $\bar{E}$ as large as 500 MeV, one might worry about sizable discrepancies between the pairing energy of the saddle configuration and that of the final fragments. Fortunately, fluctuations in the pairing energy in our results are always less than 3 MeV, so this uncertainty is negligible compared with 20 MeV. Finally, the limited region in which the receding fragments are sufficiently far apart that the asymptotic energy may be accurately estimated and yet still not too close to the mesh edge introduces an additional uncertainty in the determinations of the dissipation. However, variation of the mesh size again indicates that this error is small on the scale of 20 MeV.

The origin of the variation of fission-fragment kinetic energies with Δ is clarified by Table II. Here, one observes that the scission translational energy is virtually independent of the gap. Thus, none of the variation in the final energy can be described in terms of dissipation in the coordinate r. Rather, the variation arises primarily from the higher Coulomb interaction energy of the much more compact scission shape which occurs for large Δ. This dependence of scission elongation on the gap is particularly evident in Fig. 7. Microscopically, for small Δ, orbit occupations do not change easily and shape changes are somewhat restricted to stretching of the original shape, which necessarily creates a long neck. For large Δ, since macroscopic volume and surface energies prefer a shorter neck and more spherical fragments at each end of the dumbbell, appropriate reoccupation of single-particle levels will create such a configuration. To the degree to which

occupied orbitals in each fragment correspond more closely to ground state levels in spherical nuclei, the fission fragments will have lower excitation energy. By overall energy conservation, this lower excitation energy compensates the scission Coulomb interaction energy which eventually is transformed primarily into kinetic energy of the receding fragments.

From this discussion, it is evident that there is no fundamental relation between the gap and a classical viscosity. Although superficially, with respect to scission time and fragment kinetic energy, $1/\Delta$ does behave qualitatively the same as viscosity, the scission translational energy is essentially unaffected by Δ whereas, as shown below, it depends significantly on viscosity.

B. Macroscopic solutions

The nuclear shapes corresponding to the macroscopic solutions with various types of dissipation are shown in the four right-hand columns of Fig. 6. In each case we use a dashed line for the shape at which the neck loses stability against rupture.[35] Compared to the nonviscous case, both two-body viscosity and modified one-body dissipation lead to more elongated shapes during the descent, whereas the original one-body dissipation leads to more compact shapes. For two-body viscosity and modified one-body dissipation, the time required to reach the point of neck rupture is about 1.3 times as long as that for the nonviscous case, whereas for the original one-body dissipation it is about 5.2 times as long. With respect to both overall elongation and the time required to reach the point of neck rupture, the TDHF solution resembles the macroscopic solutions with two-body viscosity and modified one-body dissipation rather than the macroscopic solution with the original one-body dissipation.

The time required to reach the point of neck rupture is tabulated for each case in Table II, where we also give the translational kinetic energy, the vibrational kinetic energy, the dissipated energy, and the potential energy at neck rupture. The vibrational kinetic energy is the collective kinetic energy relative to the center-of-mass motion of each half of the system. The dissipated energy is equal to the time integral of twice the Rayleigh dissipation function along the dynamical trajectory. The potential energy is given relative to that for the spherical shape.

For two-body viscosity and modified one-body dissipation, the translational kinetic energy at neck rupture is about 0.7 times as large as that for the nonviscous case and is about 1.6 times as large as that for the TDHF solutions. This is to be contrasted with the original one-body dissipation, where the translational kinetic energy at neck rupture is about 0.02 times as large as that for the nonviscous case and is about 0.04 times as large as that for the time-dependent Hartree-Fock solutions.

Although the vibrational kinetic energy at neck rupture is small in all cases, the original one-body dissipation reduces it much more than does either two-body viscosity or modified one-body dissipation. For the original one-body dissipation, the dissipated energy at neck rupture is about 1.4 times as large as that for two-body viscosity or modified one-body dissipation. Compared to the value for nonviscous flow, the potential energy of deformation at neck rupture is lowered by two-body viscosity and modified one-body dissipation because of the more elongated shapes, whereas it is raised by the original one-body dissipation because of the more compact shape.

Unfortunately, the properties of the system at the point of neck rupture are not measured experimentally. To be able to compare with an experimental result, we present in Table III the calculated translational kinetic energy of the fission fragments at infinity. With the exception of the result for the original one-body dissipation, these results are calculated by approximating the motion of the fission fragments after neck rupture in terms of spheroids, as discussed in Refs. 31 and 35. For the original one-body dissipation, where the shape change after neck rupture is small, the final kinetic energy is calculated as the sum of the translational kinetic energy, Coulomb interaction energy, and nuclear interaction energy at neck rupture. The result for a nonviscous descent is 11% larger than the experimental value. The results for two-body viscosity and modified one-body dissipation agree with the experimental value to within its uncertainty. Each of these results has been calculated with a coefficient that was adjusted to reproduce optimally fission-fragment kinetic energies for the fission of nuclei throughout the Periodic Table. The result for the original one-body dissipation, which has been calculated without the introduction of any adjustable parameters, is 5% larger than the experimental value.

VI. SUMMARY AND CONCLUSIONS

Subject to the limitations of axial symmetry and the omission of the spin-orbit interaction, the time-dependent mean-field approximation has been successfully applied to the fission of ^{236}U. The resulting fission dynamics has all the expected qualitative features and, given the uncertainty in

the effective gap, is not inconsistent with the observed most probable fission-fragment kinetic energies or ternary α events. Furthermore, there exists a conceptually clear program in which, in principle, the initial adiabatic TDHF wave function provides an ensemble of initial conditions from which all fission observables may be unambiguously calculated microscopically without any free parameters.

Comparison of the constrained HF energy-of-deformation surface with macroscopic-microscopic calculations demonstrates satisfactory agreement of the two approaches once the existence of two distinct fission valleys is recognized and taken into account. Although the presence of two fission valleys is possibly an artifice of the omission of the spin orbit force, this present work suggests that a careful search should be made to determine if such an effect ever occurs in realistic situations.

Several different macroscopic descriptions of dissipation have been compared with TDHF. *A priori*, one would expect one-body dissipation to correspond most closely to the microscopic dissipation in TDHF. Thus, at first, it appears quite surprising that the original one-body dissipation formulation yields shapes, fission times, and scission parameters in Fig. 6 and Table II which differ so dramatically from those obtained in TDHF. Upon investigation, it is evident that the gross discrepancies arise primarily from the non-Galilean invariance of the original theory, and the modified one-body dissipation theory is in substantial agreement with TDHF. One surprising, and rather disappointing result is that appropriate strengths of two-body viscosity and one-body dissipation yield such similar results. Thus, the fission observables considered to date are incapable of distinguishing between two drastically different physical dissipation mechanisms.

Several significant challenges for the future arise from this work. One obvious task is to remove the symmetry restrictions in TDHF and to include the spin-orbit interaction. Short of this, at least some theoretical estimate of the effective gap is required. In addition, a conceptually clear, theoretically sound connection is required between the time-dependent mean-field theory and macroscopic approximations. Clearly, the evolution of hundreds of single-particle wave functions involves far too much specific information. What is required is a clear separation of shell effects and a smooth, underlying continuum dynamics, as in the Strutinsky approach to the static problem, and a closed set of equations relating a small number of continuum variables, such as the nucleon density and current distribution. Thus, the venerable problem of nuclear fission continues to pose significant theoretical challenges.

ACKNOWLEDGMENTS

Several of the authors are indebted to N. Glendenning for his kind hospitality and computer support at the Lawrence Berkeley Laboratory, where much of this work was carried out. In addition, P. Hoodbhoy and K.T.R. Davies made significant contributions to the development of the coordinate-space static HF and TDHF codes, respectively. We wish to acknowledge extensive discussions with H. Flocard, who has been concurrently investigating fission in collaboration with J. Blocki using a two-centered HO basis. Finally, we are grateful to W. J. Swiatecki for his critical comments concerning this manuscript, which reinforce our convictions expressed in the conclusions that many important questions remain to be resolved.

---

*This work was supported by the U. S. Energy Research and Development Administration under Contracts Nos. W-7405-ENG-36 and EY-76-C-02-3069. *000, and by the U. S. National Science Foundation under Contract No. PHY76-02724.

†Alfred P. Sloan Research Fellow.

‡Present address: Department of Mathematical Physics, University of Lund, Lund 7, Sweden.

§Present address.

[1]P. Bonche, S. Koonin, and J. W. Negele, Phys. Rev. C 13, 1226 (1976).

[2]S. E. Koonin, Phys. Lett. 61B, 227 (1976).

[3]J. A. Maruhn and R.Y. Cusson, Nucl. Phys. A270, 471 (1976).

[4]S. E. Koonin, K. T. R. Davies, V. Maruhn-Rezwani, H. Feldmeier, S. J. Krieger, and J. W. Negele, Phys. Rev. C 15, 1359 (1977).

[5]R. Y. Cusson, R. K. Smith, and J. A. Maruhn, Phys. Rev. Lett. 36, 1116 (1976).

[6]V. Maruhn-Rezwani, K. T. R. Davies, and S. E. Koonin, Phys. Lett. 67B, 134 (1977).

[7]B. Yoon and J. W. Negele, Phys. Rev. A16, 1451 (1977).

[8]S. J. Krieger, Nucl. Phys. A276, 12 (1977).

[9]J. W. Negele, in Proceedings of the Topical Conference on Heavy-Ion Collisions, Fall Creek Falls State Park, Pikeville, Tennessee, 1977 [Oak Ridge National Laboratory Report No. CONF-770602, 1977 (unpublished)], p. 73.

[10]J. Blocki and H. Flocard, Nucl. Phys. A273, 45 (1976).

[11]J. W. Negele and D. Vautherin, Phys. Rev. C 5, 1472 (1972).

[12]P. Hoodbhoy and J. W. Negele, Nucl. Phys. A288, 23 (1977).

[13]D. Vautherin and D. M. Brink, Phys. Rev. C 5, 626 (1972).

[14]J. R. Nix and W. J. Swiatecki, Nucl. Phys. 71, 1

(1965).
[15]J. R. Nix, Nucl. Phys. A130, 241 (1969).
[16]M. Baranger, in *Proceedings of the European Conference on Nuclear Physics, Aix-en-Provence, France, 1972,* [J. Phys. (Paris) 33, C5-61 (1972)]; D. M. Brink, M. J. Giannoni, and M. Veneroni, Nucl. Phys. A258, 237 (1976); M. Baranger and M. Veneroni (unpublished).
[17]F. Villars, Nucl. Phys. A285, 269 (1977).
[18]H. Flocard, Phys. Lett. 49B, 129 (1974).
[19]J. W. Negele, Comments Nucl. Part. Phys. 7, 141 (1977).
[20]H. Flocard (private communication).
[21]J. W. Negele, Nucl. Phys. A142, 225 (1970).
[22]C. T. Alonso, in *Proceedings of the International Colloquium on Drops and Bubbles, Pasadena, California*, 1974, edited by D. J. Collins, M. S. Plesset, and M. M. Saffren (California Institute of Technology, Pasadena, 1976), Vol. I, p. 139.
[23]J. A. Maruhn, T. A. Welton, and C. Y. Wong, in Oak Ridge National Laboratory Report No. ORNL-5137, 1976 (unpublished), pp. 134–137.
[24]J. A. Maruhn, in Proceedings of the Topical Conference on Heavy-Ion Collisions, Fall Creek Falls State Park, Pikeville, Tennessee, 1977 (see Ref. 9), p. 156.
[25]I. Kelson, Phys. Rev. 136, B1667 (1964).
[26]R. W. Hasse, Phys. Lett. 27B, 605 (1968).
[27]R. W. Hasse, Nucl. Phys. A128, 609 (1969).
[28]R. W. Hasse, Phys. Rev. C 4, 572 (1971).
[29]A. J. Sierk and J. R. Nix, in *Proceedings of the International Atomic Energy Agency Symposium on the Physics and Chemistry of Fission, Rochester, New York*, 1973 (International Atomic Energy Agency, Vienna, 1974), Vol. II, p. 273.
[30]J. R. Nix and A. J. Sierk, Phys. Scr. 10A, 94 (1974).
[31]K. T. R. Davies, A. J. Sierk, and J. R. Nix, Phys. Rev. C 13, 2385 (1976).
[32]A. J. Sierk and J. R. Nix, In Proceedings of the Symposium on Macroscopic Features of Heavy-Ion Collisions, Argonne, Illinois, 1976 [Argonne National Laboratory Report No. ANL/PHY-76-2, 1976 (unpublished)], Vol. I. p. 407.
[33]J. R. Nix and A. J. Sierk, Phys. Rev. C 15, 2072 (1977).
[34]A. J. Sierk and J. R. Nix, Phys. Rev. C 16, 1048 (1977).
[35]K. T. R. Davies, R. A. Managan, J. R. Nix, and A. J. Sierk, Phys. Rev. C 16, 1890 (1977).
[36]A. J. Sierk, S. E. Koonin, and J. R. Nix, Phys. Rev. C (to be published).
[37]M. Brack, J. Damgaard, H. C. Pauli, A. S. Jensen, V. M. Strutinsky, and C. Y. Wong, Rev. Mod. Phys. 44, 320 (1972).
[38]J. R. Nix, Annu. Rev. Nucl. Sci. 22, 65 (1972).
[39]P. Möller and J. R. Nix, in *Proceedings of the International Atomic Energy Agency Symposium on the Physics and Chemistry of Fission, Rochester, New York*, 1973 (see Ref. 29), Vol. I, p. 103.
[40]H. J. Krappe and J. R. Nix, in *Proceedings of the Third International Atomic Energy Agency Symposium on the Physics and Chemistry of Fission, Rochester, New York*, 1973 (see Ref. 29), Vol. I, p. 159.
[41]H. J. Krappe, Nucl. Phys. A269, 493 (1976).
[42]P. Möller and J. R. Nix, Nucl. Phys. A272, 502 (1976).
[43]P. Möller and J. R. Nix, Nucl. Phys. A281, 354 (1977).
[44]V. M. Strutinsky, Nucl. Phys. A95, 420 (1967).
[45]V. M. Strutinsky, Nucl. Phys. A122, 1 (1968).
[46]M. Bolsterli, E. O. Fiset, J. R. Nix, and J. L. Norton, Phys. Rev. C 5, 1050 (1972).
[47]W. D. Myers and W. J. Swiatecki, Nucl. Phys. 81, 1 (1966).
[48]K. T. R. Davies and J. R. Nix, Phys. Rev. C 14, 1977 (1976).
[49]P. Möller and J. R. Nix, Nucl. Phys. A229, 269 (1974).
[50]P. Möller, S. G. Nilsson, and J. R. Nix, Nucl. Phys. A229, 292 (1974).
[51]D. R. Inglis, Phys. Rev. 103, 1786 (1956).
[52]P. Möller and J. R. Nix, Nucl. Phys. (to be published).
[53]G. Wegmann, Phys. Lett. 50B, 327 (1974).
[54]D. H. E. Gross, Nucl. Phys. A240, 472 (1975).
[55]W. J. Swiatecki, in Proceedings of the International School-Seminar on Reactions on Heavy Ions with Nuclei and Synthesis of New Elements, Dubna, U. S. S. R., 1975 [Joint Institute for Nuclear Research Report No. JINR-D7-9734, 1976 (unpublished)], p. 89.
[56]J. Błocki, Y. Boneh, J. R. Nix, J. Randrup, M. Robel, A. J. Sierk, and W. J. Swiatecki, Ann. Phys. (N.Y.) (to be published).
[57]S. Koonin, R. Hatch, and J.Randrup, Nucl. Phys. A283, 87 (1977); S. Koonin and J. Randrup, *ibid.* A289, 475 (1977).
[58]H. Lamb, *Hydrodynamics* (Dover, New York, 1945), 6th ed., Sec. 329, pp. 579–581.
[59]H. Goldstein, *Classical Mechanics* (Addison-Wesley, Reading, 1959), Chap. 1, Sec. 5, pp. 19–22.
[60]L. P. Meissner, Lawrence Berkeley Laboratory Computer Center Program No. D2 BKY ZAM, 1965 (unpublished).
[61]J. A. Zonneveld, *Automatic Numerical Integration*, Mathematical Centre Tract No. 8 (Mathematisch Centrum, Amsterdam, 1964), p. 23.
[62]D. L. Hill and J. A. Wheeler, Phys. Rev. 89, 1102 (1953).
[63]B. B. Back, O. Hansen, H. C. Britt, and J. D. Garrett, Phys. Rev. C 9, 1924 (1974).
[64]D. S. Burnett, Lawrence Berkeley Laboratory Report No. UCRL-11006, 1963 (unpublished).